Pergamon

Solid-State Electronics Vol. 39, No. 11, pp. 1581–1592, 1996

PII: S0038-1101(96)00070-6
0038-1101/96 $15.00 + 0.00

LOW FREQUENCY NOISE CHARACTERISTICS OF AlInAs/InGaAs HETEROJUNCTION BIPOLAR TRANSISTORS

SHENG-LYANG JANG[1], WAY-MING CHEN[1], HAO-HSIUNG LIN[2] and CHAO-HSING HUANG[2]

[1]Department of Electronic Engineering, National Taiwan Institute of Technology, 43 Keelung Road, Section 4, Taipei 10772, Taiwan, Republic of China
[2]Department of Electrical Engineering, National Taiwan University, Taipei, Taiwan, Republic of China

(Received 27 March 1996)

Abstract—This paper studies both experimentally and theoretically the low frequency noise of AlInAs/InGaAs HBTs (heterojunction bipolar transistors). Experiments were carried out in the frequency range between 10 Hz and 100 kHz and the measured collector voltage noise consists of $1/f$ nosie and generation-recombination noise. The HBTs have finite output resistance; we have developed an experimental technique for noise measurement accounting for the finite output resistance, and present a theoretical $1/f$ noise model for the HBTs. Good agreement between the theoretical and experimental $1/f$ noises has been achieved, and it is found that at high collector current bias the measured $1/f$ collector voltage noise is due to the mobility fluctuation of carriers in the quasi-neutral emitter. Copyright © 1996 Published by Elsevier Science Ltd

1. INTRODUCTION

Low frequency noise can limit the bandwidth and stability of a wide variety of integrated circuits. It can be used as a study tool to evaluate the material property and device characteristics. Although noise has been studied for many decades, recently researchers have paid much more attention to the noise in high-speed compound devices, because the advance of technologies provides better control of material quality and thus consistent experimental results can be produced. Heterojunction bipolar transistors (HBTs) have promising ultra-high-speed digital and microwave, and milimeter-wave analog circuit applications. In terms of microwave applications, low-frequency noise, which usually has $1/f$ noise spectra, is of fundamental importance, because microwave oscillator phase noise characteristics suffer from $1/f$ noise of the devices[1]. In comparison with GaAs FETs, HBTs benefit not only from high-frequency but also from low-frequency noise performance, i.e. low $1/f$ noise[2]. The low-frequency noise observed in GaAs FET devices originates from fast trapping states that are associated with isolation by the substrate and surface effects[3]. In contrast, the base region of a BJT is screened by conducting emitter and collector tests from these surface and substate effects resulting in a lower noise. Although there have been a number studies on the low-frequency noise of HBTs[1–5], the theoretical discussions were phenomenological and were based on the theory developed for homojunction Si material. The discussions were described qualitatively, the exact location of the noise source and the nature of its relationship with the terminal voltages has not been examined in a quantitative way.

It is well established that both current gain and $1/f$ noise are affected by surface recombination current in the extrinsic base region, which is strongly influenced by the device structure and materials. By including a passivation layer at the extrinsic base region of AlGaAs HBTs, the low-frequency noise has been effectively reduced[1,4]. AlGaAs/GaAs HBTs, having relatively high surface recombination velocity, are disadvantageous in comparison with AlInAs/InGaAs HBTs and Si BJT. Therefore the AlInAs/InGaAs HBT has lower low-frequency noise[1], in particular lower $1/f$ noise. Flicker ($1/f$) noise is an excess noise found to some extent in all types of transistor and some types of resistor. Flicker noise has various origins: in Si bipolar transistors it is caused mainly by traps associated with contamination and crystal defects at the base–emitter junction; it can also be caused by the mobility fluctuation.

This paper studies the noise performance of electronic AlInAs/InGaAs HBTs fabricated by the MBE system with the goal to explore the measurement technique, to develop a theoretical HBT $1/f$ noise model, and to evaluate quantitatively the noise performance of AlInAs/InGaAs HBTs. To discuss the $1/f$ nosie model we should have a clear understanding of carrier transport; based on the thermionic emission process and the current-balancing concept we shall construct the HBT I–V and $1/f$ noise model. Since AlInAs/InGaAs HBTs have a finite value of output resistance[6], and an experimental measurement technique for extracting noise

sources is unavailable in literature, we shall discuss a measurement technique similar to that presented by Kleinpenning[7].

2. THEORY

2.1. *HBT* I–V *model*

2.1.1. Collector current. $Al_{0.48}In_{0.52}As/In_{0.53}Ga_{0.47}As$ HBT high-speed performance has been demonstrated. However, it has been noted by many researchers that InGaAs-collector HBTs typically exhibit low-common-emitter collector breakdown voltage and high output conductance, which is believed to be related to low bandgap. To reduce hot-electron injection, inserting an undoped low-band-gap spacer layer between the low-band-gap base and high-band-gap emitter was used. The main principle of this simple method is to utilize the voltage drop across the undoped spacer layer so as to supress the heterojunction spike. Figure 1 shows the energy band diagram of a double HBT with two spacer layers. The electric field, $E(x)$, in the space-charge-region (SCR) is given by Ref. [8], where:

$$E(x) = \begin{cases} \dfrac{qN_{d11}(x + x_1)}{\epsilon_1} & -x_1 \leqslant x \leqslant -\delta_1 \\ \dfrac{qN_{d11}(x_1 - \delta_1)}{\epsilon_1} + \dfrac{qN_{d12}(x + \delta_1)}{\epsilon_2} & -\delta_1 \leq x \leqslant 0 \\ \dfrac{qN_a(x_b - x)}{\epsilon_2} & 0 \leqslant x \leqslant x_b, \end{cases} \tag{1}$$

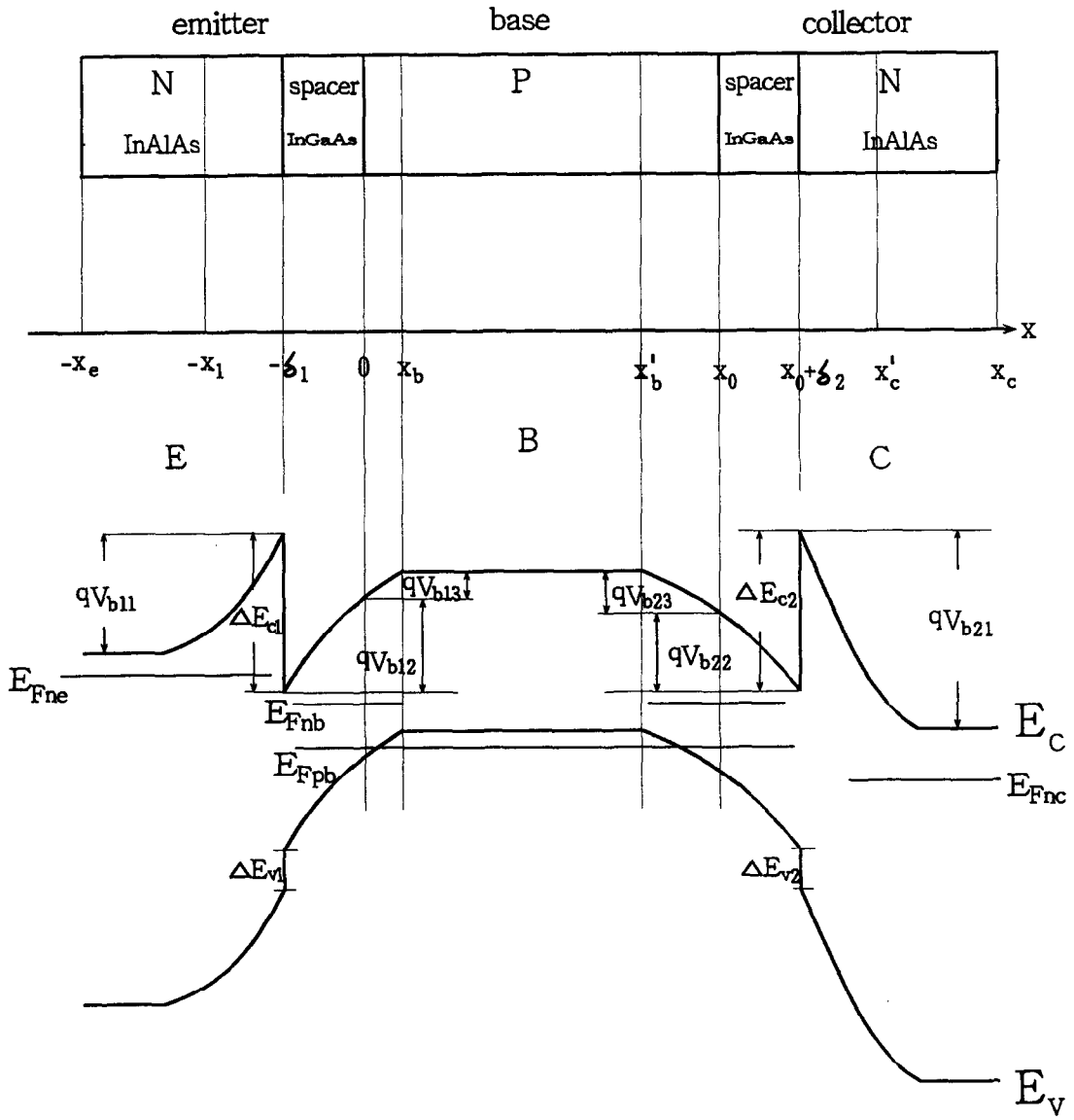

Fig. 1. The energy band diagram of HBT.

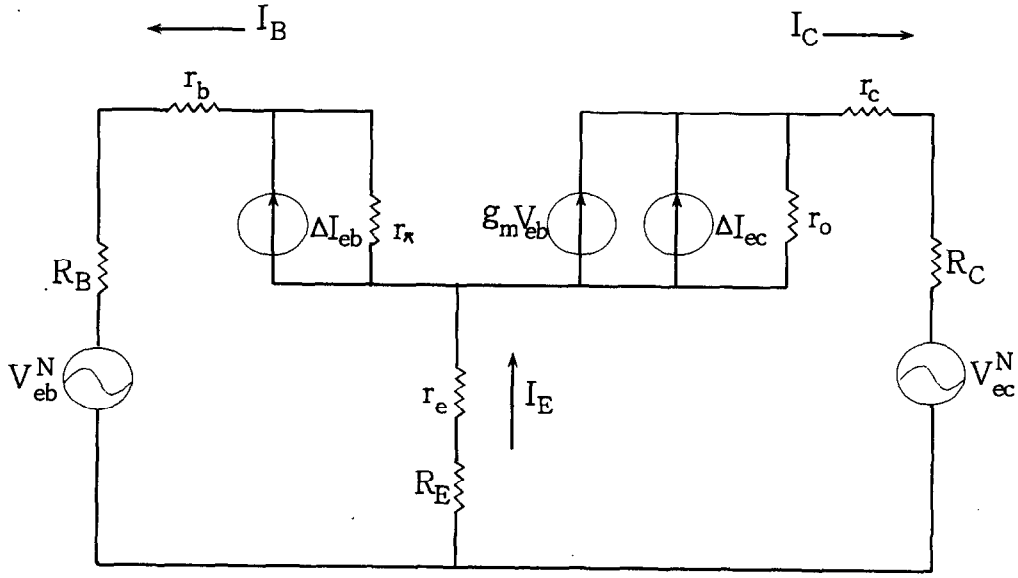

Fig. 2. Low-frequency, small-signal equivalent circuit of HBT.

where N_{d11}, N_{d12}, and N_a are the doping concentrations in the emitter, emitter spacer, and base, respectively. x_1 and x_b are the depletion widths in the emitter and base, respectively. δ_1 is the width of the emitter spacer, and ϵ_1, ϵ_2 are the permittivities of AlInAs and InGaAs, respectively. From the above equation we can get x_b, x_1, and the barrier potentials V_{b11}, V_{b12}, V_{b13}. The potential spike can be evaluated

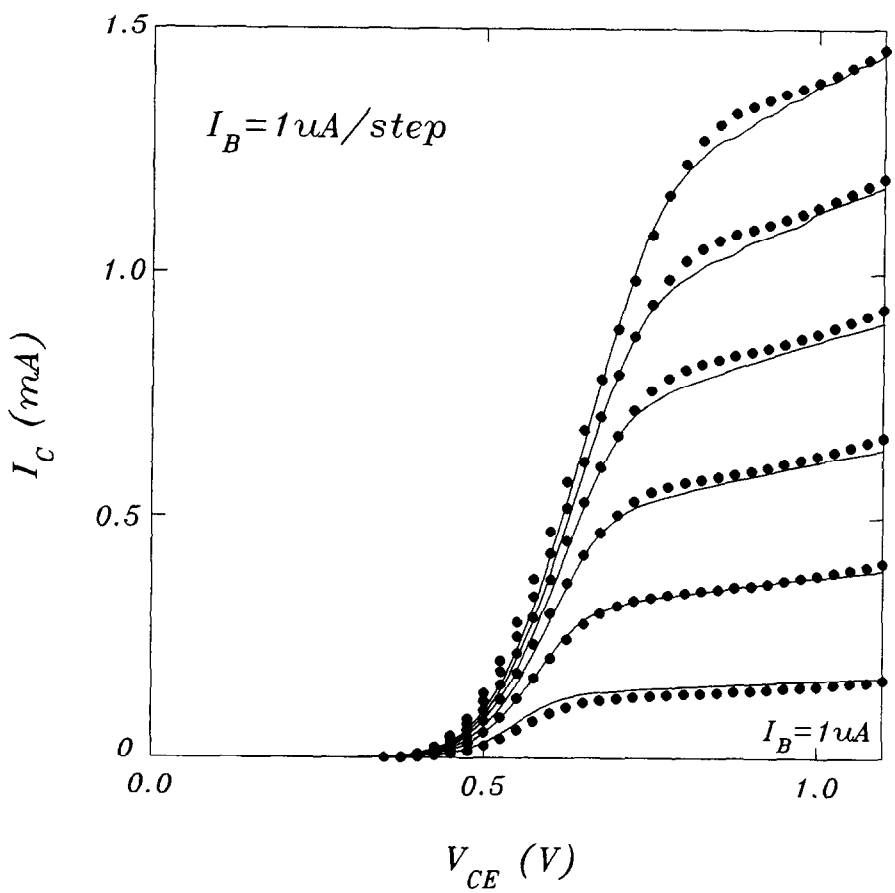

Fig. 3. Output characteristics of the AlInAs/GaInAs HBT.

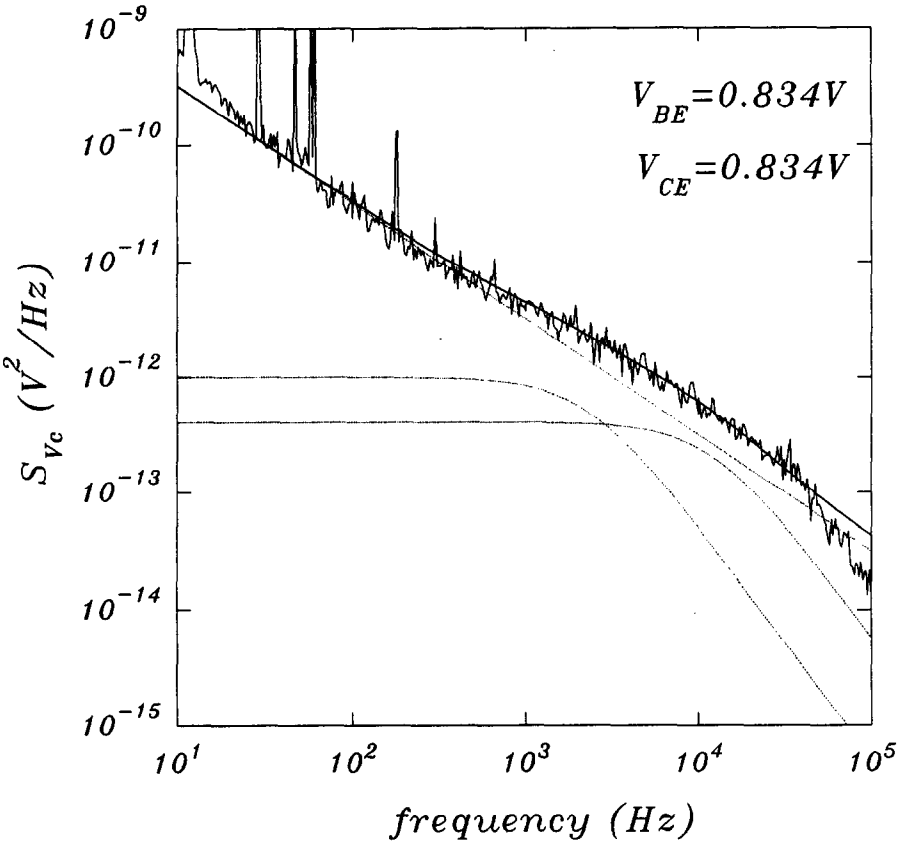

Fig. 4. Low-frequency collector voltage spectral intensity versus frequency.

by using $\Delta E_{n1} = \Delta E_{c1} - q(V_{b12} + V_{b13})$. The emitter spacer enables band bending in both conduction and valence bands. In the conduction band, it forms a deep notch at the heterointerface. This band bending enables the electron injection energy into the base to be at an optimum, and increases the hole barrier and the current gain. The applied base–emitter (BE) voltage V_{be} is related to the potential barriers by:

$$V_{bie} - V_{be} = V_{b11} + V_{b12} + V_{b13}, \tag{2}$$

where V_{bie} is the BE junction built-in potential and can be derived by using eqn (7).

The electron current density across the BE hetrojunction can be described by two opposed thermionic emission fluxes[9,10]:

$$J_n'(-\delta_1) = -qv_{n1}\left[n_e(-\delta_1^-) - \beta_1 n_b(-\delta_1^+)\exp\left(\frac{-\Delta E_{c1}}{qV_t}\right)\right], \tag{3}$$

where $v_{n1} = \sqrt{qV_t/(2\pi m_e)}$, and $v_b = \sqrt{qV_t/(2\pi m_b)}$, and $\beta_1 = m_e v_b/(m_b v_e)$. q is the electron charge, and V_t is the thermal voltage. m_e and m_b are the electron masses in the emitter and base respectively. v_e, and v_b are the electron thermal velocities in the emitter and base respectively. Assuming the quasi-Fermi levels are flat across the base and emitter SCRs, respectively, then the electron densities in the emitter (n_e) and in the base (n_b) can be written as:

$$n_e(-\delta_1^-) = n_e(-x_1)\exp\left(\frac{-V_{b11}}{V_t}\right) \tag{4a}$$

$$n_b(-\delta_1^+) = n_b(x_b)\exp\left(\frac{V_{b12} + V_{b13}}{V_t}\right). \tag{4b}$$

Substituting eqn (4) into eqn (3) yields:

$$J_n'(-\delta_1) = -q\beta_1 v_{n1} e^{(V_{b12} + V_{b13}/V_t)}\left(\frac{n_e(-x_1)}{\beta_1} \times e^{(V_{bie} + V_{be}/V_t)} - n_b(x_b)e^{(-\Delta E_{c1}/qV_t)}\right). \tag{5}$$

The electron current density given by eqn (5) is equal to the electron current density due to diffusion, $J_n'(x_b)$, given by:

$$J_n'(x_b) = -\frac{qD_{nb}}{L_{nb}} \frac{(n_b(x_b) - n_{b0})\cosh\left(\frac{W_B}{L_{nb}}\right) - (n_b(x_b') - n_{b0})}{\sinh\left(\frac{W_B}{L_{nb}}\right)} \tag{6}$$

where $W_B = x_b' - x_b$, D_{nb} the base electron diffusion coefficient, and L_{nb} the base electron diffusion length. The excess electron concentration at the base-side boundary of the BE SCR can be determined by equating (5) and (6):

$$n_b(x_b) = n_{b0} + \frac{1}{\zeta_n}\left\{\frac{\eta_n}{\beta_1}\exp\left(\frac{\Delta E_{n1}}{qV_t}\right)(n_b(x_b') - n_{b0}) + \frac{n_e(-x_1)}{\beta_1}\exp\left(\frac{-qV_{bie} + qV_{be} + \Delta E_{c1}}{qV_t}\right) - n_{b0}\right\}, \tag{7}$$

where the subscript 0 denotes the equilibrium value and

$$\eta_n = \frac{D_{nb}}{v_{n1}L_{nb}\sinh\left(\frac{W_B}{L_{nb}}\right)} \tag{8}$$

$$\zeta_n = 1 + \frac{\eta_n}{\beta_1}\cosh\left(\frac{W_B}{L_{nb}}\right)\exp\left(\Delta E_{n1}qV_t\right). \tag{9}$$

Similarly we can derive the I–V relation in the base–collector (BC) junction. The potential spike is defined as $\Delta E_{n2} = \Delta E_{c2} - q(V_{b22} + V_{b23})$. The applied BC voltage V_{bc} can be written as:

$$V_{bic} - V_{bc} = V_{b21} + V_{b22} + V_{b23}, \tag{10}$$

where V_{bic} is the BC junction built-in potential. Similar to eqn (5) the electron current density across the abrupt BC heterojunction can be written as:

$$J_n'(x_0 + \delta_2) = qv_{n2}\beta_2\exp\left(\frac{-\Delta E_{n2}}{qV_t}\right)\left(n_{b0}\left(\exp\left(\frac{V_{bc}}{V_t} - 1\right)\right) - (n_b(x_b') - n_{b0})\right), \tag{11}$$

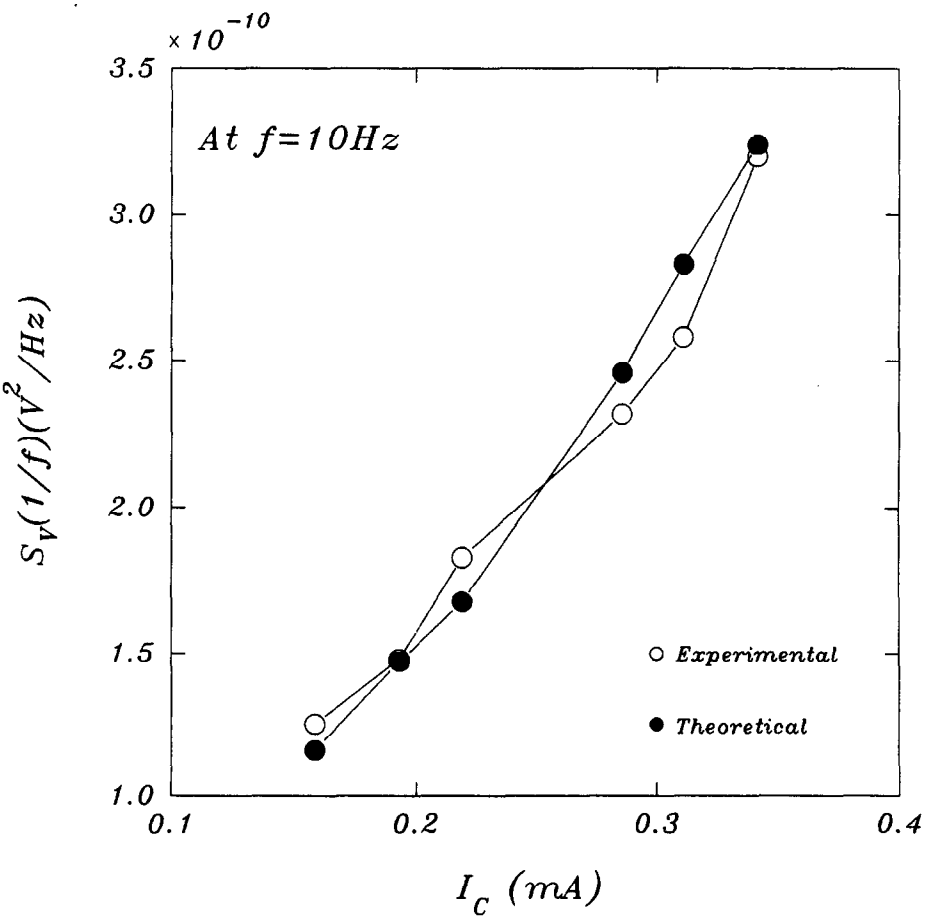

Fig. 5. Current-dependence of collector voltage $1/f$ noise at 10 Hz.

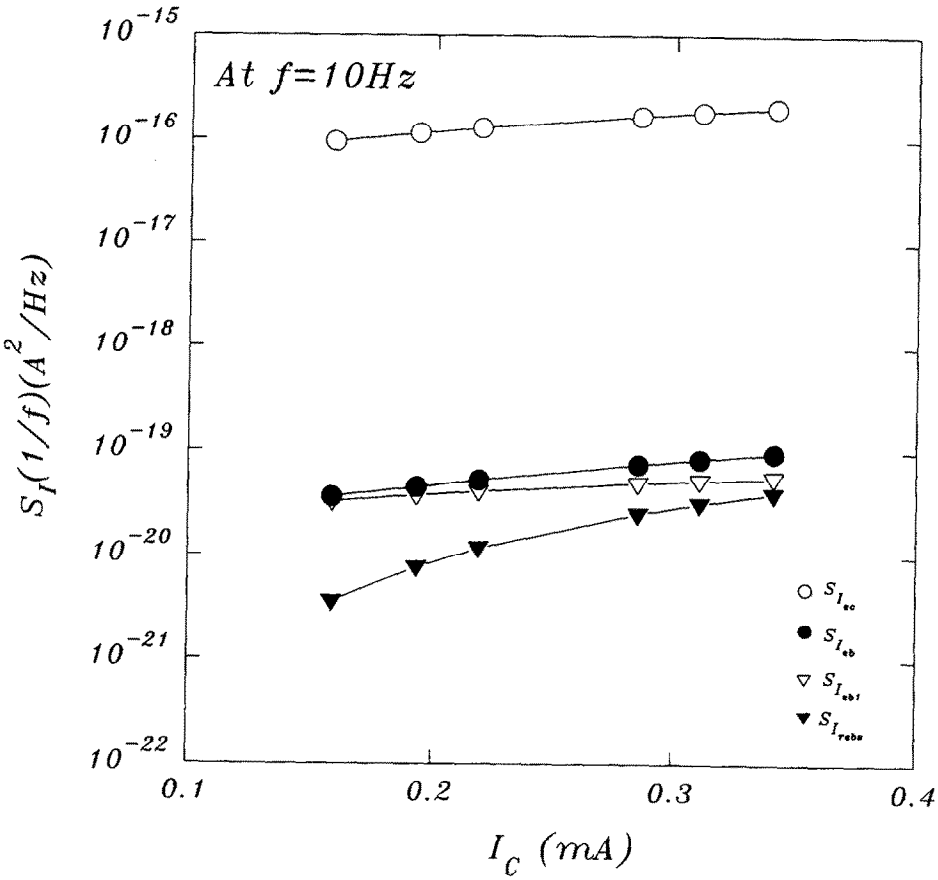

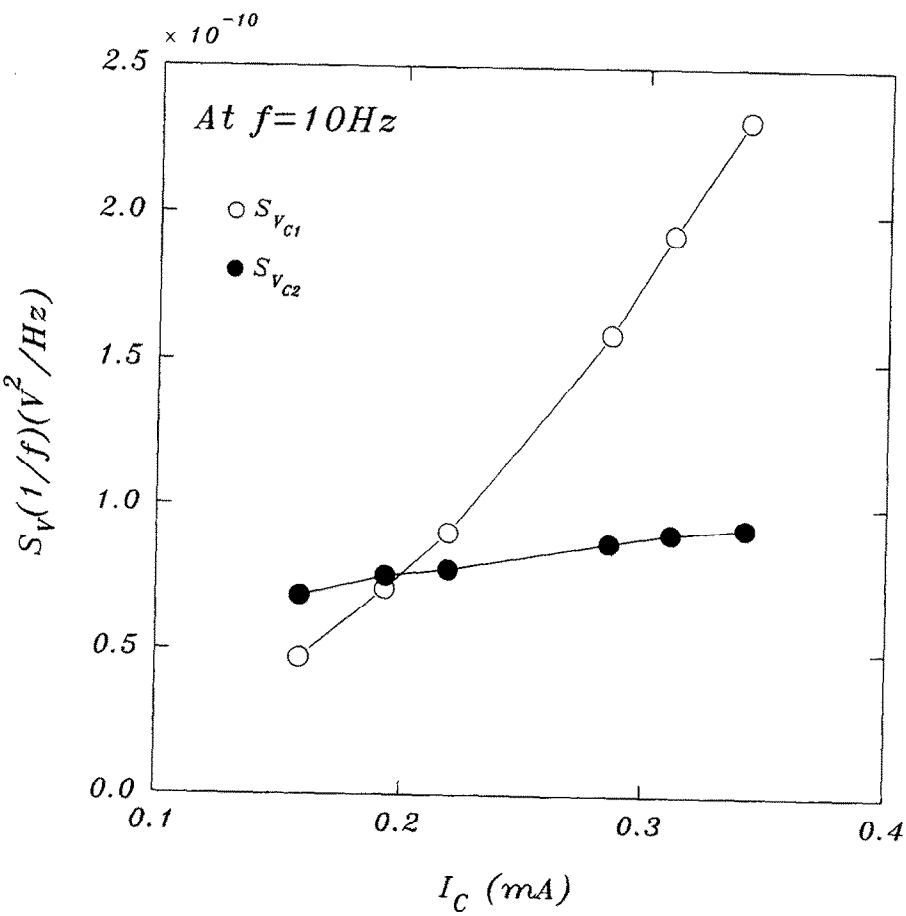

Fig. 6. (a) Current-dependence of $1/f$ nosie source at 10 Hz. (b) Determination of the dominant measured noise component.

where $v_{n2} = \sqrt{qV_t/(2\pi m_c)}$, $\beta_2 = m_c v_b/(m_b v_c)$. m_c is the collector electron mass. The electron current density given by (11) is equal to the diffusion electron current density, $J_n'(x_b')$, given by:

$$J_n'(x_b') = -\frac{qD_{nb}}{L_{nb}} \frac{(n_b(x_b) - n_{b0}) - (n_b(x_b') - (n_{b0})\cosh\left(\frac{W_B}{L_{nb}}\right)}{\sinh\left(\frac{W_B}{L_{nb}}\right)} \tag{12}$$

Substituting (7) into (12), we can get:

$$J_n'(x_b') = -\frac{qD_{nb}}{L_{nb}\sinh\left(\frac{W_B}{L_{nb}}\right)} \frac{1}{\zeta_n}\left\{\left(\frac{\eta_n}{\beta_1}\exp\left(\frac{\Delta E_{n1}}{qV_t}\right) - \zeta_n \cosh\left(\frac{W_B}{L_{nb}}\right)\right)(n_b(x_b') - n_{b0}) + \left(\frac{n_e(-x_1)}{n_{e0}\, n_{b0}}\exp\left(\frac{V_{be}}{V_t}\right) - n_{b0}\right)\right\}. \tag{13}$$

Equating (12) and (13) yields:

$$n_b(x_b') - n_{b0} = \frac{-C_3 n_{b0}\left(\exp\left(\frac{V_{bc}}{V_t}\right) - 1\right) - B_3\left(\frac{n_e(-x_1)}{n_{e0}} n_{b0}\exp\left(\frac{V_{be}}{V_t}\right) - n_{b0}\right)}{A_3 - C_3}, \tag{14}$$

where

$$\begin{cases} A_3 = q\dfrac{D_{nb}}{L_{nb}\sinh\left(\frac{W_B}{L_{nb}}\right)}\dfrac{1}{\zeta_n}\left(\dfrac{\eta_n}{\beta_1}\exp\left(\dfrac{\Delta E_{n1}}{qV_t}\right) - \zeta_n\cosh\left(\dfrac{W_B}{L_{nb}}\right)\right) \\ B_3 = q\dfrac{D_{nb}}{L_{nb}\sinh\left(\frac{W_B}{L_{nb}}\right)}\dfrac{1}{\zeta_n} \\ C_3 = qv_{n2}\beta_2\exp\left(\dfrac{-\Delta E_{n2}}{qV_t}\right). \end{cases} \tag{15}$$

Substituting (14) into (7) yields:

$$n_b(x_b) - n_{b0} = \frac{-g_n C_3 n_{b0}\left(\exp\left(\frac{V_{bc}}{V_t}\right) - 1\right) + (A_3 - C_3 - g_n B_3)\left(\frac{n_e(-x_1)}{n_{e0}} n_{b0}\mathrm{e}\left(\frac{V_{be}}{V_t}\right) - n_{b0}\right)}{\zeta_n(A_3 - C_3)}, \tag{16}$$

Table 1. Device parameters

Symbol	Value	Unit	Nomenclature
A_e	1.12×10^{-5}	cm^2	emitter area
A_c	1.0×10^{-4}	cm^2	collector area
N_{d11}	1.00×10^{17}	cm^{-3}	emitter doping
N_{d12}	9.0×10^{14}	cm^{-3}	emitter spacing doping
N_a	2.08×10^{18}	cm^{-3}	base doping
N_{d21}	1.00×10^{17}	cm^{-3}	collector doping
N_{d22}	9.0×10^{14}	cm^{-3}	collector spacer doping
N_t	6.80×10^{15}	cm^{-3}	SCR trap density
N_{ts}	1.95×10^{11}	cm^{-2}	surface state density
x_e	1.5×10^{-5}	cm	
δ_1	3.0×10^{-6}	cm	
x_0	1.50×10^{-5}	cm	
δ_2	0.08×10^{-6}	cm	
x_c	3.0×10^{-4}	cm	
R_{me}	20	Ω	emitter contact resistance
R_{mb}	29	Ω	base contact resistance

where

$$g_n = \frac{\eta_n}{\beta_1}\exp\left(\frac{\Delta E_{n1}}{qV_t}\right). \tag{17}$$

Substituting (14) into (12) gives the collector current:

$$I_c = A_e J_n'(x_0 + \delta_2) = \frac{A_e C_3 n_{b0}}{A_3 - C_3}\left[A_3\left(\exp\left(\frac{V_{bc}}{V_t}\right) - 1\right) + B_3\left(\frac{n_e(-x_1)}{n_{e0}}\exp\left(\frac{V_{be}}{V_t}\right) - 1\right)\right], \tag{18}$$

where A_e is the emitter area. Letting $\Delta E_{c2} = 0$ and assuming in the low-level injection yields the I–V model for single HBT.

2.1.2. Base current. According to the spatial distribution, there are several base current components in the HBT including (a) hole current density $J'_p(-x_1)$ injected from the base into the emitter; (b) electron–hole recombination current density J_{rebscr} in the BE SCR; (c) electron–hole recombination current density J_{rebs} in the BE surface; (d) in the saturation mode holes injected from the base into the collector and contributing to a base current component, $J'_p(x_0 + \delta_2)$. Here we limit the generation-recombination (GR) process to that through Shockley–Read–Hall (SRH) centers.

We first consider (a) the emitter recombination current density. The thermionic hole current density across the BE heterojunction reads:

$$J'_p(-\delta_1) = qv_{p1}(p_e(-x_1)e^{(V_{b11}/V_t)} - \beta_{p1}p_b(x_b)e^{(-V_{b12}-V_{b13}-\Delta E_{v1}/qV_t)}), \quad (19)$$

where $v_{pb} = \sqrt{qV_t/(2\pi m_{pb})}$, $v_{p1} = \sqrt{qV_t/(2\pi m_{pe})}$, and $\beta_{p1} = m_{pe}v_{pb}/(m_{pb}v_{p1})$. m_{pe} and m_{pb} are the hole masses in the emitter and base respectively. In equilibrium, using (19) we can get the equilibrium emitter hole density, p_{e0}. Using (2) and (19) we can get:

$$J'_p(-\delta_1) = qv_{p1}\exp\left(\frac{V_{b11}}{V_t}\right)\left[(p_e(-x_1) - p_{e0}) - p_{e0}\left(\exp\left(\frac{V_{be}}{V_t}\right) - 1\right)\right]. \quad (20)$$

We assume that at $x = -x_e$ carriers travel at the recombination velocity v_{se}, hence:

$$J'_p(-x_e) = -qv_{se}(p_e(-x_e) - p_{e0}). \quad (21)$$

The diffusion current densities in the emitter read:

$$J'_p(-x_1) = -\frac{qD_{pe}}{L_{pe}}(p_e(-x_1) - p_{e0})\cosh\left(\frac{W_E}{L_{pe}}\right) - (p_e(-x_e) - p_{e0})\sinh\left(\frac{W_E}{L_{pe}}\right), \quad (22)$$

and

$$J'_p(-x_e) = -\frac{qD_{pe}}{L_{pe}}(p_e(-x_1) - p_{e0}) - (p_e(-x_e) - p_{e0})\cosh\left(\frac{W_E}{L_{pe}}\right)\sinh\left(\frac{W_E}{L_{pe}}\right), \quad (23)$$

where $W_E = x_e - x_1$, D_{pe} the emitter hole diffusion coefficient, and L_{pe} the emitter hole diffusion length.

The excess hole concentration at the emitter side boundary of the BE SCR can now be determined by equating (20) and (22),

$$p_e(-x_1) = p_{e0} + \frac{1}{\zeta_p}\left\{\eta_p(p_e(-x_e) - p_{e0}) + p_{e0}\left(\exp\left(\frac{V_{be}}{V_t}\right) - 1\right)\right\}, \quad (24a)$$

where

$$\eta_p = \frac{D_{pe}\exp\left(\frac{-V_{b11}}{V_t}\right)}{v_{p1}L_{pe}\sinh\left(\frac{W_E}{L_{pe}}\right)}$$

$$\zeta_p = 1 + \eta_p\cosh\left(\frac{W_E}{L_{pe}}\right). \quad (24b)$$

Substituting (24a) into (23) yields:

$$J'_p(-x_e) = -\frac{qD_{pe}}{L_{pe}}\left(\eta_p - \zeta_p\cosh\left(\frac{W_E}{L_{pe}}\right)\right)(p_e(-x_e) - p_{e0}) + p_{e0}\left(\exp\left(\frac{V_{be}}{V_t}\right) - 1\right)\Big/\zeta_p\sinh\left(\frac{W_E}{L_{pe}}\right). \quad (25)$$

Setting (21) equal to (25) gives

$$p_e(-x_e) - p_{e0} = \frac{\xi_p}{\kappa_p}p_{e0}\left(\exp\left(\frac{V_{be}}{V_t}\right) - 1\right), \quad (26a)$$

where

$$\xi_p = \frac{D_{pe}}{\zeta_p v_{se}L_p\sinh\left(\frac{W_E}{L_{pe}}\right)}$$

$$\kappa_p = 1 - \xi_p\eta_p + \xi_p\zeta_p\cos\left(\frac{W_E}{L_{pe}}\right). \quad (26b)$$

Substituting (26a) into (24a) yields:

$$p_e(-x_1) - p_{e0} = \frac{1}{\zeta_p}\left\{\left(\eta_p\frac{\xi_p}{\kappa_p} + 1\right)p_{e0}\left(\exp\left(\frac{V_{be}}{V_t}\right) - 1\right)\right\}. \quad (27)$$

Substituting (27) into (19) gives the emitter recombination current density:

$$J'_p(-\delta_1) = qv_{p1}e^{(V_{b11}/V_t)}\left\{\left(\frac{1}{\zeta_p}\left(\eta_p\frac{\xi_p}{\kappa_p} + 1\right) - 1\right)p_{e0}(e^{(V_{be}/V_t)} - 1)\right\}. \quad (28)$$

Secondly we discuss (b) the BE SCR recombination current density J_{rebscr}. The SCR recombination current density in the BE SCR can be expressed by

$$J_{rebscr} = q\int_{-x_1}^{-\delta_1} U_{SHR}\,dx + q\int_{-\delta_1}^{0} U_{SHR}\,dx + \int_{0}^{x_b} U_{SHR}\,dx \quad (29)$$

where U_{SHR} is the SHR GR rate. The SRH GR process consists of four individual processes: R_a, the electron capture rate; R_b, the electron emission rate; R_c, the hole capture rate; R_d, the hole emission rate. The maximum value of U_{SHR} exists in the BE SCR[11], we approximate the SCR recombination current density by, for $V_{be} > V_t$,

$$J_{rebscr} = \int_{-x_1}^{x_b} qU_{SRH}\,dx \approx \frac{qW}{2}\sigma V_{th} N_t n_{ies}(\exp(V_{be}/(2V_t)) - 1) \quad (30)$$

where W is the thickness of the BE SCR, approximated by $(\delta_1 + x_b)$. V_{th} is the thermal velocity, σ is the trap capture cross section, N_t is the SCR trap density and n_{ies} is the emitter-spacer intrinsic carrier density.

Thirdly we develop (c) the BE surface recombination current density J_{rebs}. The surface recombination current depends on the surface state density, N_{ts}, the characteristics of the surface states and surface charge. In case $R_a \gg R_b$ and $R_c \gg R_d$, and in steady-state $v_{thn}\sigma_n \approx v_{thp}\sigma_p p$, the trap Fermi level is pinned at the trap energy level, then the surface recombination current at the surface of p–n junction perimeter is given by[12]

$$I_{rebs} \approx qW_s L_s \frac{(v_{thn}\sigma_n v_{thp}\sigma_p)^{1/2} N_{ts}(p_s n_s)^{1/2}}{2} \quad (31)$$

where W_s is the length of the perimeter of p–n junction. n_s and p_s are the electron and hole densities respectively at the surface. v_{thn}, v_{thp}, σ_n and σ_p are the electron and hole thermal velocities, and the electron and hole capture cross sections respectively. L_s is the effective length for minority carriers confined by the Coulomb attraction of the surface[12,13], and:

$$n_s p_s = n_{ies}^2 \exp\left(\frac{qV_{be}}{KT}\right). \quad (32)$$

The net base current is written as:

$$I_b = A_e J_p'(-\delta_1) + A_e J_{rebscr} + I_{rebs} + A_c J_p'(x_0 + \delta_2) \quad (33)$$

where $J_p'(x_0 + \delta_2)$ is in a similar form as $J_p'(-\delta_1)$. A_c is the collector area. The ideality factor of the junction surface recombination current was shown to have a value ≈ 2, whereas the ideality factor is ≈ 1 for the extrinsic base recombination current[14,15].

2.2. *Physical basis for noise measurement*

Figure 2 shows the low-frequency, small-signal equivalent circuit of HBTs and its bias circuit, where R_B, R_C, and R_E are respectively the external base, collector and emitter resistances; r_b, r_e, and r_c are respectively the intrinsic base, collector and emitter resistances; g_m is the transconductance, r_π is the input base resistance, where $g_m r_\pi = \beta(h_{FE})$, β is the current gain. ΔV_{eb}^N is the Nyquist noise for R_B, r_b, R_E, and r_e, ΔV_{ce}^N is the Nyquist noise for R_B, r_b, R_C, and r_c. From the Kirchoff current law we can get:

$$\Delta I_E = \Delta I_B + \Delta I_c \quad (34)$$

$$\Delta I_B = \Delta I_{eb} + \frac{\Delta V_{eb}}{r_\pi} \quad (35)$$

$$\Delta I_C = \Delta I_{ec} + g_m \Delta V_{eb} + \frac{\Delta V_{ec}}{r_0} \quad (36)$$

where r_0 is the output resistance of the HBT and can be calculated. Δ represents the fluctuation. Using the Kirchoff voltage law we can get

$$\Delta V_{eb} = -(R_B + r_b)\Delta I_B - I_B \Delta r_b - (R_E + r_e)\Delta I_E - I_E \Delta r_e + \Delta V_{eb}^N \quad (37)$$

$$\Delta V_{ec} = -(R_C + r_c)\Delta I_C - I_C \Delta r_c - (R_E + r_e)\Delta I_E - I_E \Delta r_e + \Delta V_{ec}^N \quad (38)$$

From the above equations we can get:

$$\Delta I_C = \frac{-\beta\xi R\Delta I_{eb} + (r_\pi + R\xi)\Delta I_{ec}}{Z} + \frac{\beta\Delta V_{eb}^N + \eta\Delta V_{ec}^N}{Z} - \frac{((r_\pi + R\xi)/r_0) I_C \Delta r_c + ((r_\pi + R\xi)/r_0 + \beta) I_E \Delta r_e + \beta I_B \Delta r_b}{Z}, \quad (39a)$$

where

$$\begin{cases} \beta(h_{FE}) = g_m r_\pi \\ \eta = \dfrac{r_\pi + R\xi}{r_0} \\ \xi = \dfrac{\beta R_0}{\beta r_0 - (R_E + r_e)} \\ R = R_B + r_b + R_E + r_e + \dfrac{R_E + r_e}{g_m r_0} \\ Z = \left[1 + \dfrac{R_C + r_c + R_E + r_e}{r_0}\right] \\ \quad \times (r_\pi + R\xi) + \beta(R_E + r_e). \end{cases} \tag{39b}$$

From the above equation we can arrive at the collector voltage spectral density:

$$S_{V_c} = \frac{(\beta\xi R)^2 S_{I_{eb}} + (r_\pi + R\xi)^2 S_{I_{ec}}}{(Z/R_C)^2} + \frac{(\eta I_C)^2 S_{r_c} + ((\eta + \beta) I_E)^2 S_{r_e} + (\beta I_B)^2 S_{r_b}}{(Z/R_C)^2} + \frac{\beta^2 S_{V_{eb}^N} + \eta^2 S_{V_{ec}^N}}{(Z/R_C)^2} \tag{40}$$

As can be seen, the collector voltage noise is affected by the current noise sources $S_{I_{eb}}$ and $S_{I_{ec}}$ the one associated with BC junction is neglected because the BC junction is reverse-biased and the BC current is negligible. It is also affected by the noises (S_{r_e}, S_{r_b}, S_{r_c}) generated in the series resistances. The above equations show that S_{V_c} is a function of both intrinsic noise sources as well as the equivalent circuit parameters.

2.3. 1/f *noise origins*

Both bulk- and surface-related mechanisms for $1/f$ noise have been suggested, we therefore develop the HBT $1/f$ noise model similar to the developed noise model[16,17] for homojunction devices.

2.3.1. Model of surface-velocity fluctuation 1/f *noise.* The surface recombination current due to surface state density N_{ts} is:

$$I_{rebs} = qA_{eff} W_x v_{thp} \sigma_p N_t' f_t p_s, \tag{41}$$

where $A_{eff}(= W_s L_s)$ is the effective recombination surface area. f_t is the occupancy factor. N_t' is the trap density. We define W_x by $N_{ts} = N_t' W_x$. The total number of charged interface states D_{it} is defined by:

$$D_{it} = A_{eff} N_{ts}^- = A_{eff} f_t N_{ts}. \tag{42}$$

We can express the current as a steady-state term plus a fluctuation term, then:

$$I_{rebs} = I_{rebs0} + \Delta I_{rebs} = I_{rebs0} + qv_{thp}\sigma_p(p_s - N_t'^-)\Delta D_{it}, \tag{43}$$

where we have assumed $\Delta p_s/W_x + \Delta N_{ts}^- = 0$. If the statistical event of the deviation ΔD_{it} from the average value D_{it} are independent of each other, then[16]:

$$\overline{\Delta D_{it}^2} = \overline{[A_{eff}\Delta N_t'^-]^2} = A_{eff} f_t (1 - f_t) N_{ts}. \tag{44}$$

Combining (43) and (44) yields:

$$\overline{\Delta I_{rebs}^2} = I_{rebs}^2 \left(\frac{p_s - N_t'^-}{p_s}\right)^2 \frac{1 - f_t}{A_{eff} N_{ts} f_t}. \tag{45}$$

Following Van der Ziel's treatment[16], the spectral intensity of carrier number fluctuation can be defined by:

$$S_{D_{it}} = \overline{4\Delta D_{it}^2} \int_0^\infty \frac{\tau g(\tau) d\tau}{1 + (\omega\tau)^2} \tag{46}$$

where

$$g(\tau)d\tau = \begin{cases} \dfrac{d\tau}{\tau \ln(\tau_1/\tau_0)} & \tau_0 \leqslant \tau \leqslant \tau_1 \\ 0 & \text{otherwise.} \end{cases} \tag{47}$$

Since the surface state current is mostly generated by states near the Fermi-level, f_t is taken as 1/2. If $1/\tau_0 \gg \omega \gg 1/\tau_1$, from (45) we can get:

$$S_{I_{rebs}} = I_{rebs}^2 \left(\frac{p_s - N_t'^-}{p_s}\right)^2 \frac{1}{N_{ts} A_{eff}} \frac{1}{\pi f \ln(\tau_1/\tau_0)}. \tag{48}$$

$S_{I_{rebs}}$ is the base current spectral density due to the fluctuation current ΔI_{rebs}. Using $R_a = R_c$ and (32) we can get:

$$p_s = \left(\frac{v_{thn}\sigma_n}{v_{thp}\sigma_p}\right)^{1/2} n_{ies} \exp\left(\frac{V_{be}}{2V_t}\right). \tag{49}$$

Substituting (49) into (48) we can get $S_{I_{rebs}}$.

2.3.2. Model of mobility fluctuation 1/f *noise.* The mobility fluctuation results in the collector current fluctuation ΔI_{ec}[16] from which we can get the collector current spectral density, $S_{I_{ec}}$ given by

$$S_{I_{ec}} = \frac{1}{W_B^2} I_c \frac{qD_{nb}\alpha_{nb}}{f} \ln\left(\frac{n(x_b)}{n(x_b')}\right), \tag{50}$$

where α_{nb} is the electron Hooge parameter in the base, f is the frequency. The base current spectral density $S_{I_{eb1}}$, due to the fluctuation current $\Delta I_{eb1}(I_{eb1} = A_e J_p'(-x_1))$, is:

$$S_{I_{eb1}} = \frac{1}{W_E^2} I_{b1} \frac{qD_{pe}\alpha_{pe}}{f} \ln\left(\frac{p(-x_1)}{p(-x_e)}\right), \tag{51}$$

where α_{pe} is the hole Hooge parameter in the emitter. The net base current spectral density $S_{I_{eb}}$ is $S_{I_{eb1}} + S_{I_{rebs}}$.

3. EXPERIMENTAL AND THEORETICAL RESULTS

This section describes the DC I–V characteristics and low-frequency noise performance of the InAlAs/InGaAs SHBTs, which were grown by molecular beam epitaxy[18]. The output characteristics are shown in Fig. 3. The circled lines are the experimental results, and the solid lines are the fitting results. During the noise measurement, the HBTs were shielded in a metal case to avoid external interference and biased in a common-emitter configuration. The collector was biased in series with a metal-film resistor, the collector voltage is taken out from the collector of the HBT. The collector voltage noises were then fedback to a low-noise amplifier and a PC-controlled spectrum analyzer was used to measure the noise spectrum output from the amplifier. All the experiments were carried out at room temperature. Figure 4 is the collector voltage, spectral intensities at a bias. The noise consists of a $1/f$ noise and G–R noise components.

In Fig. 4, we decompose the noise in terms of its component, and a best fitting for the curve measured at the bias condition of $V_{BE} = 0.834$ V and $V_{BC} = 0.0$ V is as follows:

$$S_{V_c}(f) = \frac{C_1}{f} + \frac{g_1}{1 + \left(\frac{f}{f_{t1}}\right)^2} + \frac{g_2}{1 + \left(\frac{f}{f_{t2}}\right)^2} + C_x \quad (52)$$

where f_{t1} and f_{t2} are the roll-off frequencies of G–R noises, and we found $C_1 = 3.2 \times 10^{-9}$, $g_1 = 1.0 \times 10^{-12}$, $f_{t1} = 2300$ Hz, $g_2 = 4.1 \times 10^{-13}$, $f_{t2} = 12{,}000$ Hz, and $C_x = 5.0 \times 10^{-15}$. Similarly we can extract the parameters at other biases. Figure 5 depicts the bias-dependence of the $1/f$ noise evaluated at $f = 10$ Hz and $V_{BC} = 0.0$ V. The unfilled circle line is the experimental result, and the filled circle line is the fitting result; as seen the trend of the theoretical result is quantitatively the same as the experimental result.

To locate the noise source, we plot $S_{I_{eb}}$ (including its components $S_{I_{rebs}}$ and $S_{I_{ebj}}$) and $S_{I_{ec}}$ versus I_c in Fig. 6(a). We found $S_{I_{eb}} \ll S_{I_{ec}}$, the noise source in the quasi-neutral base region is larger, however the base-emitter junction noise $S_{I_{eb}}$ is amplified and the base–collector $1/f$ noise $S_{I_{ec}}$ is not amplified. In Fig. 6(b), we plot $S_{V_{C1}} = (\beta\xi R R_C/Z)^2 S_{I_{eb}}$ and $S_{V_{C2}} = (r_\pi + R\xi)R_C/Z)^2 S_{I_{ec}}$ of eqn (40) versus the collector current, it is obvious that at high collector current the former term is dominant in the collector voltage noise spectral density, S_{V_C}. The collector voltage noise results from the fluctuation of charged surface states in the emitter-base surface and the mobility fluctuation in the quasi-neutral emitter, and the latter is dominated. At low collector current, the current gain is reduced and the mobility fluctuation in the quasi-neutral base is dominated. This indicates that the bias-dependent circuit elements play a very important role in determining the measured noise.

In the theoretical calculation the band-edge discontinuities for a heterojunction are given by[20,21] $\Delta E_c = 0.72\Delta E_g$ and $\Delta E_v = 0.28\Delta E_g$. The energy band gap for $Al_{0.48}In_{0.52}As$ is $E_g = 1.45$ eV and the energy band gap for $Ga_{0.47}In_{0.53}As$ is $E_g = 0.75$ eV. The mobility and diffusion constant are as in Ref. [22]: $\mu_n = 13800\ cm^2/(Vs)$ for $In_{0.53}Ga_{0.47}As$ and $D_n = 40\ cm^2/s$, $D_p = 9\ cm^2/s$ for AlInAs. The other device parameters used in the device model are listed in Table 1. The fitting Hooge parameters: $\alpha_{nb} = 1.2 \times 10^{-5}$ and $\alpha_{pe} = 7 \times 10^{-6}$, fall into the regime of reported values[19].

4. CONCLUSION

It has been shown[2] that the AlInAs/InGaAs HBTs have lower low-frequency noise compared with AlGaAs/GaAs HBTs; the comparison was based on the same measurement technique for AlGaAs/GaAs HBTs. However the AlInAs/InGaAs HBTs have a high output conductance and AlGaAs/GaAs HBTs have a very low output conductance, we can not ignore the effect of the output resistance on the measurement data. This work has developed the measurement technique by including the effect of output resistance in the small-signal equivalent circuit using a thermionic-emission HBT I–V model and extracted device parameters. It also presents formulas for the $1/f$ noise sources in the HBTs. By combining the $1/f$ noise source model with the small-signal equivalent circuit, we can calculate the $1/f$ collector-voltage noise. Fitting the theoretical $1/f$ noise with the measured $1/f$ noise, a good agreement has been achieved, and we found the noise source for the measured $1/f$ collector voltage noise locates at the quasi-neutral emitter at high collector current bias, and at the quasi-neutral base at low collector current bias.

Acknowledgements—This work was supported by the National Science Council, Taiwan, R.O.C. under Contract NSC 84-2215-E011-006.

REFERENCES

1. N. Hayama and K. Honjo, *IEEE Trans. Electron. Devices* **39,** 2180 (1992).
2. S. Tanaka, H. Hayama, A. Furukawa, T. Baba, M. Mizuta and H. Honjo, *Electron. Lett.* 1439 (1990).
3. S. C. Jue, D. J. Day, A. Margittai and M. Svilans, *IEEE Trans. Electron. Devices* **36,** 1020 (1989).
4. D. Costa and J. S. Harris, *IEEE Trans. Electron. Devices* **39,** 2383 (1992).
5. X. N. Zhang, *et al. IEEE Trans. Electron. Devices Lett.* **EDL-5,** 277 (1984).
6. R. J. Malik *et al. IEEE Trans. Electron. Devices Lett.* **EDL-5,** 277 (1984).
7. T. G. M. Kleinpenning, *IEEE Trans. Electron. Devices* **39,** 1501 (1992).
8. H. R. Chen *et al. IEEE Trans. Electron. Device Lett.* **15,** 336 (1994).

9. S. S. Perlman and D. L. Feucht, *Solid-St. Electron.* **7,** 911 (1964).
10. A. A. Grinberg, M. S. Shur, R. J. Fischer and H. Morkoc, *IEEE Trans. Electron. Devices* **ED-31,** 1758 (1984).
11. S. M. Sze, *Physics of Semiconductor Devices*. Wiley (1981).
12. S. Tiwari, *Compound Semiconductor Device Physics*. Academic Press (1992).
13. C. H. Henry, R. A. Logan and F. R. Merritt, *J. Appl. Phys.* **49,** 3530 (1978).
14. W. Liu and J. S. Harris, *IEEE Trans. Electron. Devices* **39,** 2726 (1992).
15. W. Liu and S.-K. Fan, *IEEE Trans. Electron. Devices Lett.* **13,** 510 (1992).
16. A. van der Ziel, *Noise in Solid State Devices and Circuits*. John Wiley, New York (1986).
17. N. Siabi-Shahrivar *et al. Solid-St. Electron.* **38,** 389 (1995).
18. Chao-Hsing Huang and Hao-Hsiung Lin, *Solid-St. Electron.* **36,** 1229 (1993).
19. M. Tacano, *Solid-St. Electron.* **34,** 917 (1991).
20. D. F. Welch *et al. J. Appl. Phys.* 3176 (1984).
21. R. People *et al. Appl. Phys. Lett.* 118 (1983).
22. J. J. Liou *et al. Solid-St. Electron.* **36,** 819 (1993).